

## Article

# Management of Agricultural Water Containing Acetimidothioic Acid Pesticide through Catalytic Oxidation to Facilitate Reclaimed Water Recycling for Sustainable Food Production

Ehssan Ahmed Hassan <sup>1,2,\*</sup>, Maha A. Tony <sup>3,4</sup>, Hossam A. Nabwey <sup>3,5,\*</sup>  and Mohamed M. Awad <sup>5,6</sup> 

- <sup>1</sup> Department of Biology, College of Science and Humanities, Prince Sattam Bin Abdul Aziz University, Alkharj 11942, Saudi Arabia
- <sup>2</sup> Department of Zoology, Faculty of Science, Suez Canal University, Ismailia 41522, Egypt
- <sup>3</sup> Basic Engineering Science Department, Faculty of Engineering, Menoufia University, Shebin El-Kom 32511, Egypt
- <sup>4</sup> Advanced Materials/Solar Energy and Environmental Sustainability (AMSEES) Laboratory, Faculty of Engineering, Menoufia University, Shebin El-Kom 32511, Egypt
- <sup>5</sup> Department of Mathematics, College of Science and Humanities in Al-Kharj, Prince Sattam Bin Abdulaziz University, Al-Kharj 11942, Saudi Arabia
- <sup>6</sup> Department of Mathematics, Faculty of Science, Suez Canal University, Ismailia 41522, Egypt
- \* Correspondence: e.basiouny@psau.edu.sa (E.A.H.); eng\_hossam21@yahoo.com (H.A.N.)

**Abstract:** Agro-industrial discharge contains acetimidothioic acid, which is commercially named “Lanox 90” and is a widely applied insecticide in greenhouses, and the result is wastewater loaded with this insecticide. Treating such wastewater is a must to reduce the environmental impact as well as to facilitate the opportunity for water recycling. Thus, the present work introduced Montmorillonite (MMT) clay as a novel Fenton reaction source to treat wastewater loaded with Lanox 90 insecticide as a benign sustainable strategy. Scanning electron microscopy (SEM) supported with energy-dispersive X-ray spectroscopy (EDX) and Fourier-transform infrared spectroscopy (FTIR) were used to characterize the MMT sample. Response surface methodology based on Box–Behnken analysis was selected to optimize the parametric circumstances. The optimized parameters of the proposed technique were obtained at a pH of 2.6 with the addition of 0.8 and 854 mg/L of MMT and H<sub>2</sub>O<sub>2</sub>, respectively, to attain the highest predicted Lanox 90 removal rate of 97%. Analysis of variance (ANOVA) was used to examine the statistical data and displayed a significant quadratic model. Ultimately, the results reveal that the oxidation system is exothermic and has a non-spontaneous nature, and the reaction kinetics are categorized according to the second-order reaction kinetic rate. The results of the current study indicate the importance of MMT for treating wastewater. These results confirm the possibility of using oxidation technique as a suitable candidate for greenhouse effluent management to enhance the efficiency of water recycling for smart irrigation.

**Keywords:** agricultural wastewater; water recycle; Montmorillonite; Fenton oxidation; catalyst recycle



**Citation:** Hassan, E.A.; Tony, M.A.; Nabwey, H.A.; Awad, M.M. Management of Agricultural Water Containing Acetimidothioic Acid Pesticide through Catalytic Oxidation to Facilitate Reclaimed Water Recycling for Sustainable Food Production. *Processes* **2023**, *11*, 792. <https://doi.org/10.3390/pr11030792>

Academic Editor: Antoni Sánchez

Received: 8 February 2023

Revised: 5 March 2023

Accepted: 6 March 2023

Published: 7 March 2023



**Copyright:** © 2023 by the authors. Licensee MDPI, Basel, Switzerland. This article is an open access article distributed under the terms and conditions of the Creative Commons Attribution (CC BY) license (<https://creativecommons.org/licenses/by/4.0/>).

## 1. Introduction

Nowadays, there is a persistent need for culturing through greenhouses due to the need for fruits and vegetables that are out of season. This technique assures protected conditions of crops to attain a high-quality yield. Additionally, the requirement of sustainable agricultural technology motivates the development of improved advanced greenhouses [1]. Such technology includes the enhancement in infrastructure to reclaim water in a semi-closed recycling system for the double benefits of conserving natural resources and the treatment of waste effluents to attain a sustainable food production world through efficient use of hydric resources [2]. The persistent existence of pesticides in greenhouse effluents causes grave environmental damage and raises concerns even at miniscule concentrations. In this regard, the pertinent option is to treat agricultural effluent wastewater [3].

Lanox 90, or S-methyl-N((methylcarbamoyl)oxy) thioactimidate, is signified as one of the most widely applied insecticides in greenhouse farming for the protection of ornamental plants. In this context, water is loaded with Lanox 90. Lanox 90 is one of the members of the carbamate family and is characterized by a main functional group of  $-NH(CO)O-$ . Such functional group principally attributes to its high solubility in water, which reaches 57.9 g/L (at 20 °C), and low affinity for soils [4]. These combined characteristics make it noxious for both surface and groundwater and cause damage to the ecosystem. Therefore, the World Health Organization (WHO) as well as the Environmental Protection Agency, USA (EPA), have signified it as a restricted very toxic and hazardous material.

The so-called conventional treatment methodologies, including biological treatments and physical separation through membranes, are insufficient for insecticide elimination due to the recalcitrant and bio-accumulative characteristics of insecticides [5]. To reach an acceptable quality of processed water, the search for an efficient way of treatment is engaging both the academia and the industrial world. In recent years, great attention has been paid toward dealing with active light processes called advanced oxidation systems, which are based on complete mineralization [6]. Such systems are able to oxidize pollutants to obtain risk-free end products of  $CO_2$ ,  $H_2O$ , and inorganics compounds. Photo-Fenton reaction is one of the advanced oxidation systems that is based on the production of ( $\cdot OH$ ) radicals, which are categorized as highly reactive species as a result of the interaction between  $H_2O_2$  and iron-based salts under ultraviolet illumination through a cyclic reaction to reach pollutant oxidation. This system has shown promising results in the removal of agricultural effluents containing pesticide according to the literature [6,7]. Although a high yield of Fenton's reaction is attained, the disadvantages also have to be taken into consideration. These disadvantages include the reaction precursors are expensive as well as the reaction needs a fixed pH. Additionally, the final iron sludge is a concern [8].

Currently, great efforts are focused on the improvement of photocatalysis through changing catalysts' characteristics to enhance the efficiency of their photocatalytic activity. Aluminum and iron metal are considered to be the most abundant metallic elements on the Earth's crust. Due to its chemical properties and amorphous nature, Montmorillonite, which contains aluminum, iron, and silicon, and has a porous structure and a high specific surface, is considered a replacement of iron precursors in the Fenton's reaction, specially due to its nature occurrence, which helps in reducing the operating cost. Such material is an excellent adsorbent material, although, to date, it has not been used as a source of photocatalytic reaction [9].

Response surface methodology (RSM) is a powerful scheme for photocatalytic process optimization that includes multiple variables [4,8,10]. Such methodology is applied to explore the most effective parameters in a catalytic reaction, especially in a Fenton process, since it is a multivariable dependent reaction. A 3-level factorial design, or the so-called Box–Behnken design, is a statistical model that provides a powerful experimental tool and has been increasingly applied to optimize Fenton's parameters [11,12]. This optimization tool plays a key role in the success of the photo-Fenton system. Nevertheless, it has not been well exploited to optimize Montmorillonite-based Fenton reaction.

MMT has been applied as a catalyst/adsorption source according to previous data cited in the literature [9]. However, MMT has not been used as a catalytic source to initiate the Fenton reaction, especially in the treatment of pesticide-loaded wastewater from agricultural streams. MMT in the Fenton's reaction leads to a greener photocatalytic reaction for the Fenton's test. Thus, the current investigation is a preliminary project dealing with oxidation by the photo-Fenton reaction based on the use of MMT as a naturally abundant clay for treating synthetic waters polluted via one of the most extensively applied pesticides in greenhouse farming; MMT is used as a novel Fenton's source from an environmentally benign material. An analysis of the removal of the pesticide while mineralizing its intermediates and an evaluation of the final effluent toxicity with the remaining pesticide were performed for the purpose of recycling the reclaimed water for greenhouse plants' use. Additionally, the reaction parameters were optimized to maximize toxin removals.

## 2. Experimental Materials and Methodology

### 2.1. Experimental Materials

#### 2.1.1. Lanox 90 Aqueous Effluent

Lanox 90 (L90) was applied in the current study as a commercial-grade insecticide to simulate wastewater effluent from greenhouses. L90 was supplied by an agricultural insecticide and chemical company and applied as received without further modification or treatments. The synthetic wastewater was created by preparing a stock of the aqueous solution (1000-ppm) of L90, which was then subjected to dilution, as required, to attain various L90 concentrations. Thereafter, the desired concentration was used and subjected to ultraviolet treatments at a volume of 100 mL.

#### 2.1.2. Montmorillonite-Based Photo-Fenton Catalyst

Montmorillonite, which is a naturally abundant clay substance, was selected to be the source of aluminum metal to substitute for iron in the photo-Fenton reaction. MMT was collected from the Eastern Desert in the upper part of Egypt near El Minia city at the location coordinates of 28° north and 30° east. In this regard, MMT was collected from the deposit, and the clay was taken to the laboratory for preparation by drying in an electric furnace (105 °C) for seven days to maintain it dry and to remove any excess moisture. Consequently, MMT was exposed to grinding through a ball mill to attain an acceptable powder material. The resulting powder was used as the source of the Fenton's catalyst.

### 2.2. Experimental Methods

#### 2.2.1. Wastewater Treatment Test

Acetimidothioic acid, which is commercially referred to as Lanox 90, was purchased from a central agricultural pesticide and chemical company, El-Menoufia, in Egypt. The synthetic acetimidothioic acid (Lanox 90) aqueous medium (100 mL) was poured into a 250 mL container, and certain amounts of MMT and hydrogen peroxide (30% *w/v*) as the sources of the photocatalyst were added to the container prior to being subjected to ultraviolet (UV) illumination. The pH of the aqueous Lanox 90 matrix was found to be 7.2, which was then adjusted, when needed, to the needed values through the addition of diluted H<sub>2</sub>SO<sub>4</sub> or NaOH solutions, which were of analytical grade and were supplied by Sigma-Aldrich, Darmstadt, Germany. The solution was then magnetically stirred to keep the suspension homogenous and the catalyst well dispersed. Then, the solution was periodically analyzed to investigate L90 removals. Figure 1 summarizes the treatment steps and the suggested treatment sequence.

#### 2.2.2. Experimental Design

Response surface methodological analysis (RSM) was applied to optimize the complex system's performance based on the Box–Behnken (BB) design. The BB design was selected as a multivariate nonlinear model for optimizing the response surface that influenced the system's variables, namely H<sub>2</sub>O<sub>2</sub>, MMT catalyst concentrations, and pH of the aqueous medium. These variables were chosen to investigate their effects on Lanox 90 oxidation as a dependent response.

#### 2.2.3. Kinetic Modeling

In order to investigate the kinetics of Lanox 90 oxidation in wastewater using the modified Fenton oxidation technique, the data were regressed based on the simple zero (Equation (1)), first (Equation (2)), and second (Equation (3)) kinetic orders [12] as follows:

$$\left(\frac{dc}{dt}\right) = -k_0 \quad (1)$$

$$\left(\frac{dc}{dt}\right) = -k_1C \quad (2)$$

$$\left(\frac{dc}{dt}\right) = -k_2C^2 \quad (3)$$

where  $C$  is the Lanox 90 concentration in wastewater;  $C_t$  is the Lanox 90 concentration in wastewater at time  $t$ ;  $C_0$  is the initial concentration of Lanox 90 organics in wastewater, and  $t$  is the reaction time. Additionally,  $k_0$ ,  $k_1$ , and  $k_2$  represent the kinetic rate constants of the zero-, first- and second-order reaction kinetics, respectively. Then, integrating Equations (1)–(3) leads to the linearized solutions for the zero, first, and second kinetic orders, as displayed in Equations (4)–(6), respectively.

$$(C_t = C_0 - k_0t) \quad (4)$$

$$((C_t = C_0 - e^{k_1t}) \quad (5)$$

$$\left(\frac{1}{C_t}\right) = \left(\frac{1}{C_0}\right) - k_2t \quad (6)$$

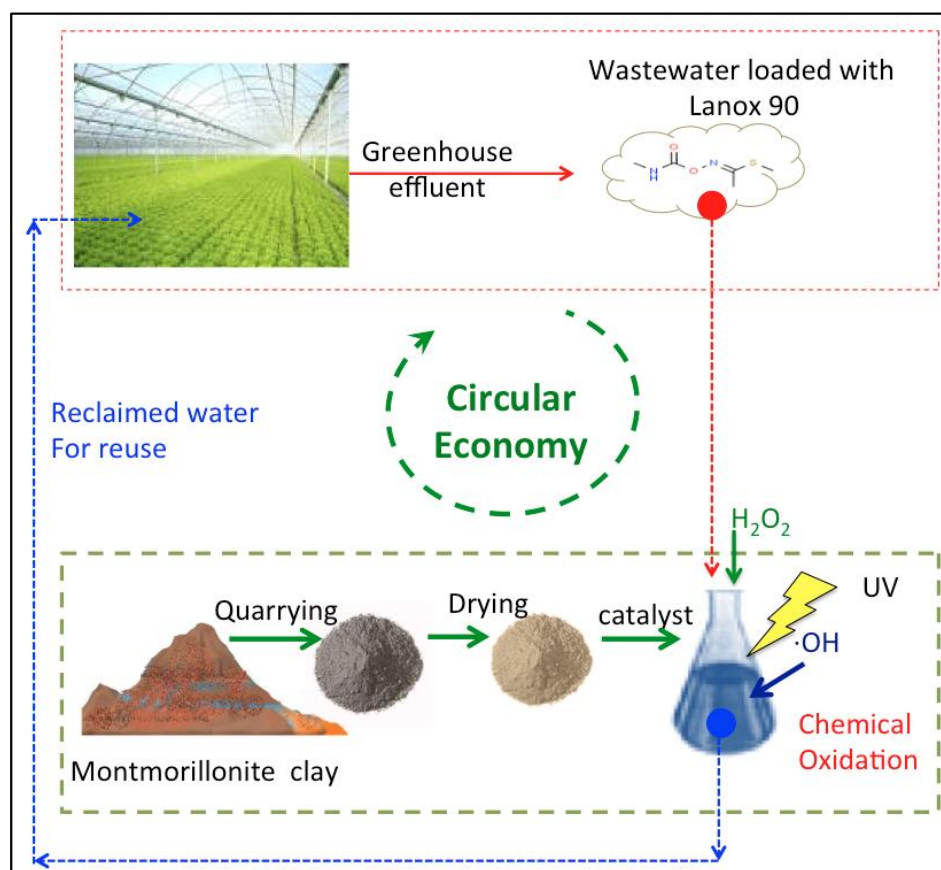


**Figure 1.** Graphical representation of agricultural wastewater effluent management.

### 2.3. Analytical Methods

The Lanox 90 solution containing the catalyst after treatment was subjected to periodic analysis at the time intervals of 10 min each. L90 was inspected in the solution at the maximum wavelength of 231 nm using a UV–visible spectrophotometer (model, Unico UV-2100 spectrophotometer, Columbus, OH, USA). The solution was kept under the photocatalytic equipment test till a steady state was achieved or complete Lanox 90 removal was attained. Prior to analysis, the catalyst was removed from the aqueous matrix through filtration using syringe filters with a size of 0.45 mm. Additionally, the pH of the aqueous solution was examined and adjusted when required using a digital pH meter (model AD1030, Adwa instrument, Szeged, Hungary).

#### 2.4. Statistical Analyses

Statistical software (SAS Institute, New York, NY, USA, V STAT 15.1) was used to investigate the full matrix of the factorial experimental design. Moreover, the Mathematica software (V 5.2) was applied to investigate the optimal numerical variables. To further understand the effect of the interacting variables and their response, surface analysis was conducted to analyze the affinity of such interactions. The 3-D response surface and 2-D contour plots were created using the MATLAB R2017a software. Moreover, to check the model, ANOVA was performed to examine the pattern and the acceptance of the model. The ANOVA results, including the sum of squares, mean squares, estimated coefficient, standard error, and the corresponding  $F$ -value and  $p$ -values were examined using a  $t$ -test. Generally, an RSM model is accepted as a significant model if its  $F$ -value is greater than the critical value while the  $p$ -value is small ( $<0.05$ ). Moreover, the  $R^2$  (the coefficient of determination) is also used to confirm the fitness of the examined model. In RSM statistics, a model is accepted when  $R^2 > 80\%$  [7].

#### 2.5. Characterization Study

The morphology of the sample (MMT) was examined and imaged using a field-emission scanning electron microscope (SEM) (FE-SEM, Quanta FEG 250, The Netherlands). The applied magnifications were  $\times 8000$  and  $\times 60,000$ . This was augmented with energy-dispersive X-ray spectroscopy (EDX) to investigate the main oxides present in the MMT sample via an examination of the energy-dispersive spectrum. Additionally, Fourier-transform infrared spectroscopy (FTIR) (Jasco, FT/IR-4100, type A, Tokyo, Japan) of the MMT sample was carried out to investigate the kind of functional group responsible for the photocatalytic reaction.

### 3. Results and Discussions

#### 3.1. Characterization of Montmorillonite Catalyst

##### 3.1.1. SEM Images of Montmorillonite

The scanning electron microscopic (SEM) images were investigated to highlight the morphology of the naturally occurring catalyst. The scanning electron micrographs of the MMT sample indicate its morphology at different magnifications. Figure 2 shows that the layered structure of the material has a smooth surface with agglomerated regularly shaped particles, which have an average particle size in the range of  $3.514 \mu\text{m}$ . The MMT surface signifies the existence of a lot of asymmetric open pores with voids. Additionally, the chemical elemental composition showing the weight ratio of the main elements on the surface was examined via an energy-dispersive X-ray spectroscopy test (EDX). The results of the elemental analysis displayed in Table 1 show that MMT possesses mainly  $\text{SiO}_2$ . Additionally, the presence of the oxides of  $\text{Al}_2\text{O}_3$  and  $\text{Fe}_2\text{O}_3$  is observed, showing its importance as a Fenton source. Such results are in accordance with what has been previously reported by various authors [9,12,13] for this type of clay mineral. The Fenton reaction could be conducted through various metals, especially iron and aluminum, which initiate the reaction. The presence of iron and aluminum oxides react with hydrogen peroxide and produce OH radicals, which drive the oxidation of Lanox 90 molecules. In addition, the surface morphology of the clay leads to the occurrences of adsorption in combination with the oxidation reaction. Additionally, a low loss of ignition (L.O.I.) value (6%) indicates the presence of organic matter and carbonate content, as well as combined water in the MMT clay. These results show the suitability of the material to be a catalyst and an adsorbent surface due to the presence of voids as well as the increase in surface area of the substance, according to the ignition of organic matter.

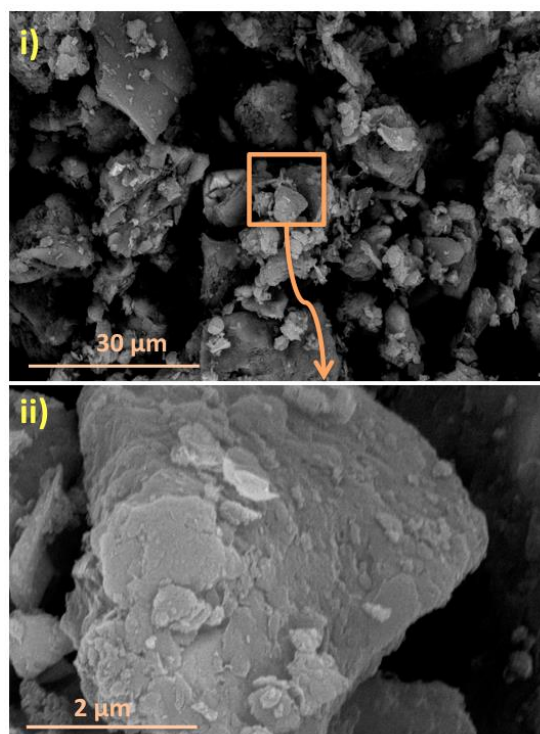


**Figure 2.** SEM images of the Montmorillonite (MMT) sample at different magnifications: (i) 4000× and (ii) 50,000×.

**Table 1.** Chemical constituents of Montmorillonite as inferred by EDX \*.

Oxides	SiO <sub>2</sub>	Al <sub>2</sub> O <sub>3</sub>	Fe <sub>2</sub> O <sub>3</sub>	CaO	MgO	K <sub>2</sub> O	Na <sub>2</sub> O	SO <sub>3</sub>	L.O.I.
Weight %	62.3	18.2	10.1	4.0	1.0	1.0	0.09	0.02	6.0

\* L.O.I.: Loss of Ignition.

### 3.1.2. FTIR Spectroscopy of Montmorillonite

Fourier-transform infrared (FTIR) transmittance spectrum analysis is a significant technique for identifying the existence of different forms of minerals; MMT as a source of photocatalyst was analyzed for its FTIR performances. Due to the presence of numerous elements, besides the presence of the main intensive absorption bands of clay, there are considerable coupled vibrations. Si–O stretching vibrations (silanol) are observed at 1032.6 cm<sup>−1</sup>, identifying the existence of quartz [13]. Furthermore, the Montmorillonite spectra show bands at 528.4 cm<sup>−1</sup> and 781.9 cm<sup>−1</sup> that are related to the stretching vibrations representing Si–O–Al group, which might validate the presence of illite [14,15]. The interlayer hydrogen bonding at 3694.9 cm<sup>−1</sup>, 3438.4 cm<sup>−1</sup>, and 1638.2 cm<sup>−1</sup> indicates the probability of hydroxyl linkage. The band at 1032.6 cm<sup>−1</sup> verifies the existence of illite. The band near 781.9 cm<sup>−1</sup> is attributed to the presence of Al–Mg–OH bonding. This spectrum confirms the presence of “Montmorillonite” clay [16]. Additionally, Al bonding is present at 820 cm<sup>−1</sup> in the spectrum, and Si–O–Fe bonding is present at 446.1 cm<sup>−1</sup> [16].

## 3.2. Lanox 90 Oxidation

### 3.2.1. Assessment of Various Oxidation Processes

The effects of various oxidation systems on Lanox 90 treatment were evaluated and compared with the MMT-based Fenton system to investigate its efficacy in removing Lanox 90 from greenhouse wastewater. The results in Figure 3 show that in the absence of MMT, while the used H<sub>2</sub>O<sub>2</sub> is recorded to be 800 mg/L, the extent of Lanox 90 oxidation barely reaches 24%. However, by solely using MMT, the decrease in Lanox 90 load is around 60% within 50 min of irradiation time. Such results show the influence of the adsorption

equilibrium due to the existence of CaO, MgO, and illite, which possess porous adsorption surfaces. However, the addition of Montmorillonite augmented with UV irradiance leads to a removal rate of 76%, confirming the role of the material as a photocatalyst. Additionally, MMT combined with H<sub>2</sub>O<sub>2</sub> shows a removal rate of 91%; this verifies the role of dark Fenton test in Lanox 90 oxidation. In order to better understand the oxidation capability, further combination of Montmorillonite/H<sub>2</sub>O<sub>2</sub>/UV oxidation was checked, and the oxidation efficiency reaches 97% of Lanox 90 removals. These results might be because of the augmentation of the sorption and photocatalytic systems [17,18].

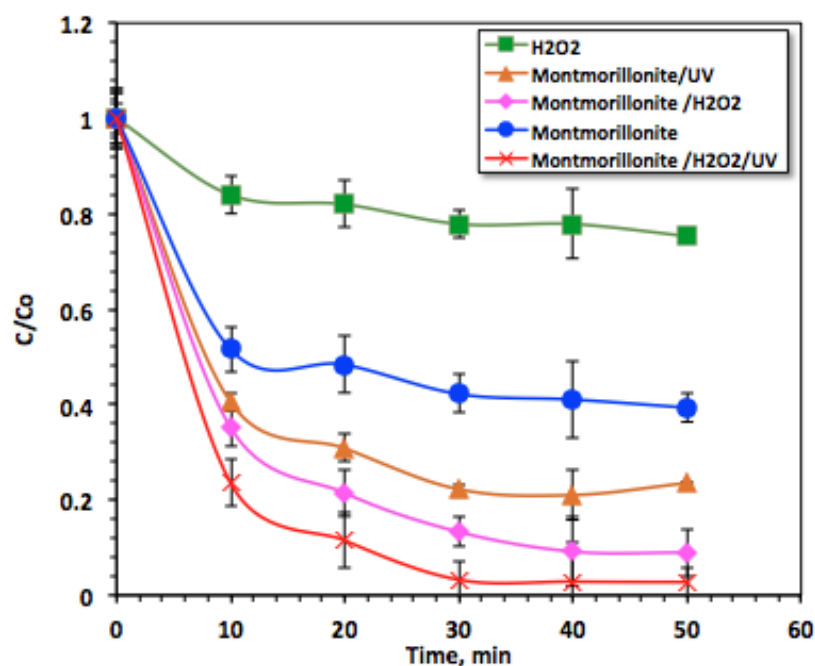


**Figure 3.** Effects of different oxidation systems on Lanox 90 elimination.

Even though hydrogen peroxide is considered a powerful oxidant, the oxidation of Lanox 90 is not significant when using this reagent. However, when Montmorillonite/H<sub>2</sub>O<sub>2</sub> is augmented with UV, the excited Lanox 90 molecules convert O<sub>2</sub> to O<sub>2</sub><sup>•</sup> since Lanox 90 absorbs ultraviolet light. Then, the autoprotolysis of H<sub>2</sub>O generates protons, which then leads to O<sub>2</sub><sup>•</sup> radicals to produce superoxide radicals (OOH<sup>•</sup>). Such radicals could ultimately completely oxidize Lanox 90 molecules to harmless end products, including CO<sub>2</sub> and H<sub>2</sub>O, as well as mineral acids [18]. The catalytic oxidation reaction of Lanox 90 molecules in the existence of Montmorillonite, under UV illumination, commonly incorporates the separation of electron/hole pairs existing on Montmorillonite and subsequent reduction–oxidation reactions. The adsorbed molecular O<sub>2</sub> species might scavenge electrons and H<sub>2</sub>O or adsorbed Lanox 90 molecules, which could trap the holes. Subsequently, L90 insecticide molecules could be oxidized directly by the effect of photogenerated oxidants. Additionally, H<sub>2</sub>O<sub>2</sub> addition in the presence of Montmorillonite and ultraviolet illumination enhances the photodegradation rate of L90 since the direct dissociation of H<sub>2</sub>O<sub>2</sub> under UV illumination produces OH<sup>•</sup> radicals, which could oxidize L90 molecules to CO<sub>2</sub>, H<sub>2</sub>O, and mineral acids [19].

### 3.2.2. Tailoring Montmorillonite for the Fenton-Based System

#### Effect of Lanox 90 Loading

The effect of initial Lanox 90 insecticide concentration in the aqueous effluent on oxidation by the Montmorillonite photo-Fenton system is shown in Figure 4. The initial H<sub>2</sub>O<sub>2</sub> concentration was added (800 mg/L) to the MMT catalyst loading that was kept at 1 g/L at a pH of 3.0. The maximum L90 removal efficiency was attained at 97% oxidation

after 50 min for the Lanox 90 loading of 50, 100, 200, and 400 mg/L. The removal efficacy of Lanox 90 reduced slowly when the Lanox 90 loading was increased, and the oxidation of L90 ranged from 99 to 71% as the Lanox 90 loading increased in the solution. This could be attributed to the quantity of MMT and  $H_2O_2$  being constant in the low (50 mg/L) and high concentrations (400 mg/L); thus,  $H_2O_2$  and MMT, which are the main elements accountable for the formation of highly oxidized  $\bullet OH$  radicals, were categorized as not being sufficient to generate enough hydroxyl radicals. Additionally, the amount of vacant active sites on the MMT surface was not sufficient to adsorb higher initial L90 loads in the aqueous matrix. The high loads of L90 occupying the active sites of MMT could result in a decline of reactive  $\bullet OH$  radicals. Numerous authors [20,21] have reported a similar trend when treating various pollutants via catalytic oxidation systems.

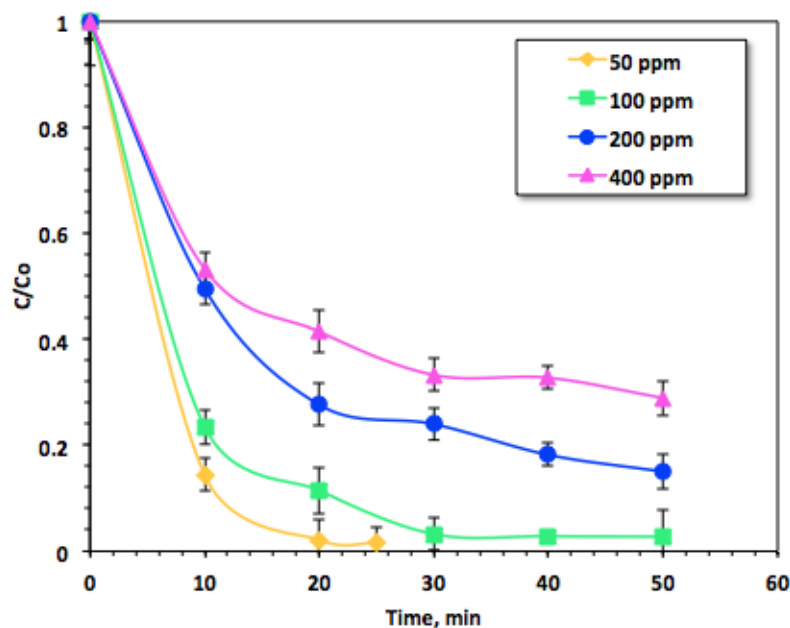


**Figure 4.** Effect of initial Lanox 90 loading on the Montmorillonite photo-Fenton oxidation system.

#### Effect of Montmorillonite Concentration

To further investigate the effect of MMT on the photo-Fenton system, the influence of its concentration was investigated, and the results are shown in Figure 5. The MMT concentration was changed over the range of 0.5 to 1.5 g/L, whereas all the other variables were kept at constant values (pH of 7.2 and  $H_2O_2$  at 800 mg/L). The oxidation tendency increases with increasing catalyst concentration, while further catalyst concentration increase results in a reduction in the oxidation efficacy, which reaches almost complete removal (98%) when 1.0 g/L of MMT was added to the aqueous matrix. Additionally, Al and Fe ions react with hydrogen peroxide to form more highly reactive hydroxyl radicals and metals ions. Such non-selective hydroxyl radicals attack the Lanox 90 molecules and strongly mineralize them. However, further increase in MMT leads to a reduction in the treatment efficacy due to the shadowing effect in the media. Excess MMT causes a turbid solution, which prevents ultraviolet radiation from penetrating the aqueous matrix and obeys the UV transmittance. Additionally, extreme metal ions that are in excess in the medium act as a scavenger of hydroxyl radicals rather than as a generator [5].

#### Effect of $H_2O_2$ Concentration

Hydrogen peroxide's effect on Lanox 90 removal in the Montmorillonite-based photo-Fenton system was investigated by varying the hydrogen peroxide concentration, and the results of the experiments are displayed in Figure 6. As expected, elevating the  $H_2O_2$  concentration from 100 mg/L to 400 mg/L enhances Lanox 90 oxidation. However, further elevation in the reagent to an optimal concentration (800 mg/L) results in a reduction in the

treatment efficacy. The oxidation declines to 83% when the  $\text{H}_2\text{O}_2$  concentration increases to more than 800 mg/L. Thus, 800 mg/L is recorded as the optimal  $\text{H}_2\text{O}_2$  concentration. This could be because excessive dosing of such reagent leads to a decline in Lanox 90 treatment since perhydroxyl radical ( $\text{HO}_2$ ) is generated due to excess hydrogen peroxide, rather than highly oxidized OH radicals. Thus, the overall oxidation rate is reduced.

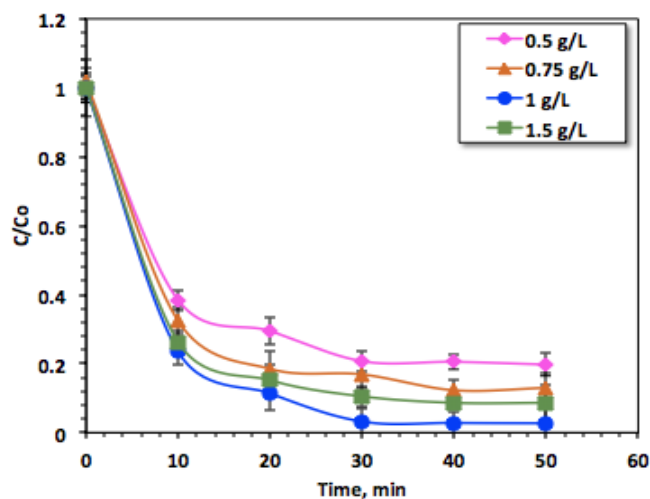


Figure 5. Effect of Montmorillonite catalyst concentration on the photo-Fenton reaction.

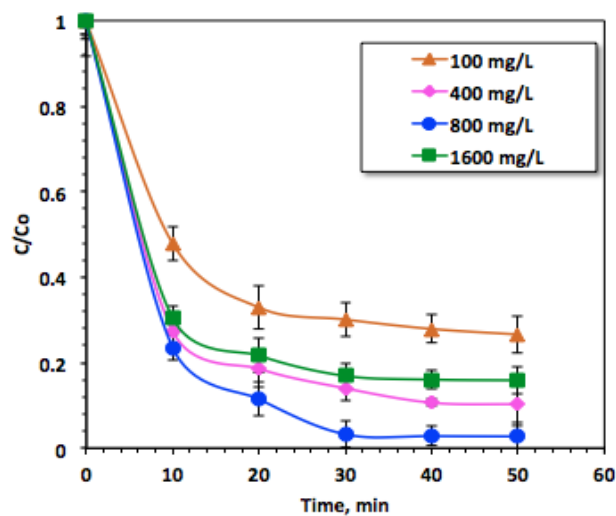


Figure 6. Effect of  $\text{H}_2\text{O}_2$  concentration on the photo-Fenton system.

#### Effect of Aqueous Effluent pH

pH is categorized as a significant variable in the photo-Fenton reaction since pH affects  $\text{H}_2\text{O}_2$  decomposition and hydrolytic speciation of metal ions. Hence, to evaluate the effect of the aqueous environment's pH on oxidation, the initial pH values of the aqueous matrix were varied from 3.0 to 7.2, and the data are expressed as a decline in Lanox 90 concentration. Figure 7 verifies that an acidic pH (3.0) shows a maximum oxidation of Lanox 90 efficiency. It is important to note that the pH value of the aqueous solution achieves the highest oxidation efficacy, which reaches 97%, during 50 min of UV irradiation and that Lanox 90 is almost totally oxidized into different intermediates. Increasing the pH value results in the creation of radicals that inhibit the oxidation reaction, instead of the generation of highly oxidized (OH) radicals. Additionally, the yield of Lanox 90 removal could be associated with the fraction of soluble metals that are responsible for inducing  $\text{H}_2\text{O}_2$  to produce (OH) radicals in the aqueous medium, which declines within an acidic pH range [9,22].

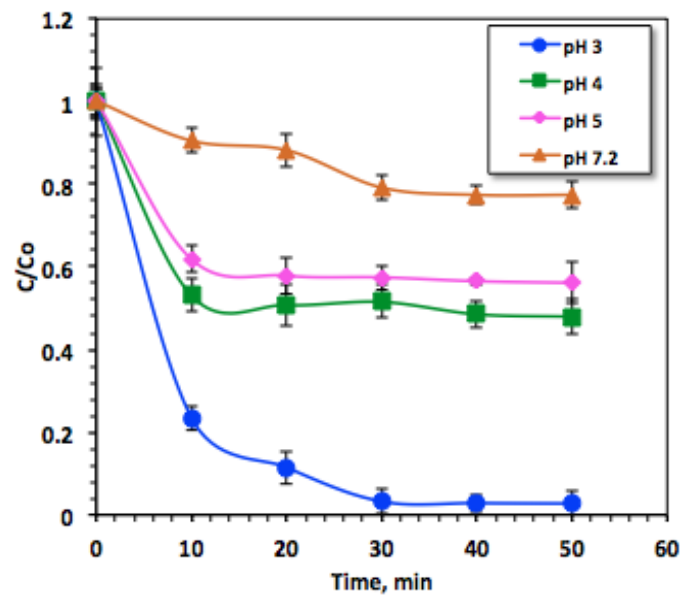


Figure 7. Effect of pH of the aqueous matrix on the photo-Fenton system.

### 3.2.3. RSM Model's Optimization of Operating Parameters Model Establishment

To attain a higher removal efficiency in a reasonable time with a minimal concentration of reagents, the 3-level factorial design, also known as the Box–Behnken model design, was correlated. A Box–Behnken design based on RSM with triplicates at the central values was applied. The following independent variables were chosen: (i)  $\text{H}_2\text{O}_2$  concentration; (ii) MMT catalyst concentration; and (iii) pH value. Their levels were selected as a support of the introductory work, and the selected levels are displayed in Table 2.

Table 2. Boundaries of model design for the coded and natural experimental domains and the corresponding levels' spacing.

Experimental Variable	Symbols		Range and Levels		
	Natural	Coded	−1	0	1
$\text{H}_2\text{O}_2$ (mg/L)	$\varepsilon_1$	$\zeta_1$	700	800	900
MMT (mg/L)	$\varepsilon_2$	$\zeta_2$	0.75	1.0	1.25
pH	$\varepsilon_3$	$\zeta_3$	2.0	3.0	4.0

Furthermore, the analysis using the SAS software suggested the full matrix of the factorial experimental design, as seen in Table 3, at the coded and un-coded levels. A 15-factorial design was performed, and the second-order polynomial model was investigated according to Equation (7):

$$Y(\%) = 92.66 + 3.62\varepsilon_1 - 6.255\varepsilon_2 - 3.875\varepsilon_3 - 6.456\varepsilon_1^2 + \varepsilon_1\varepsilon_2 - 9.75\varepsilon_1\varepsilon_3 - 5.20\varepsilon_2^2 + 4.0\varepsilon_2\varepsilon_3 - 14.45\varepsilon_3^2 \quad (7)$$

where  $Y$  is the predicted Lanox 90 removal rate depending on the parameters' response (%);  $i = 1, 2, 3$  and  $j = 1, 2, 3$ ;  $\beta_0$ ,  $\beta_i$ ,  $\beta_{ii}$ , and  $\beta_{ij}$  are the model regression coefficient variables; and  $\zeta_i$  is the input used to calculate the coded variable. In order to simplify the model calculations, the natural parameters of the operating system ( $\varepsilon_i$ ) were converted to coded variables ( $\zeta_i$ ).

#### ANOVA Test

An ANOVA test was applied to evaluate the model. The  $R^2$  and  $p$ -value were recorded to investigate the model's adequacy. A small  $p$ -value of 0.008 is obtained. Moreover, the  $R^2$  is 96%, which supports the proposed model. Thus, a good correlation is achieved for the

predicted model of Lanox 90 removal through the modified photo-Fenton test. Such results are in agreement with the previous work of Elsayed and his co-workers [10], who found a correlation coefficient of 99% for their optimized parameters for the oxidation of dye species using a chitin biopolymer system. Additionally, they recorded a  $p$ -value of 0.00054 for their model. Additionally, Nour et al. [7] found a  $p$ -value of 0.027552, which is accepted for significance of their suggested model that optimizing the variables using RSM model.

**Table 3.** Box–Behnken factorial design in terms of coded and natural variables and the corresponding Lanox 90 removal rate affecting effluent oxidation.

Exp. No.	Variables						Response (Y)
	H <sub>2</sub> O <sub>2</sub> Concentration		MMT Concentration		pH Value		% L90 Removal
	Coded	Natural	Coded	Natural	Coded	Natural	
1	−1	700	−1	0.75	0	3.0	82
2	−1	700	1	1.25	0	3.0	72
3	1	900	−1	0.75	0	3.0	88
4	1	900	1	1.25	0	3.0	82
5	0	800	−1	0.75	−1	2.0	92
6	0	800	−1	0.75	1	4.0	71
7	0	800	1	1.25	−1	2.0	67
8	0	800	1	1.25	1	4.0	62
9	−1	700	0	1.0	−1	2.0	60
10	1	900	0	1.0	−1	2.0	86
11	−1	700	0	1.0	1	4.0	77
12	1	900	0	1.0	1	4.0	64
13	0	800	0	1.0	0	3.0	92
14	0	800	0	1.0	0	3.0	93
15	0	800	0	1.0	0	3.0	93

### Response Surface Plots

The 3-D response surface and 2-D contour plots of Lanox 90 removal efficacy are displayed in Figures 8–10, showing the three pairs of selected variables. According to the data displayed in Figures 8–10, Lanox 90 removal efficacy steadily increases with an elevation in both H<sub>2</sub>O<sub>2</sub> and MMT catalyst. This could be attributed to the presence of highly reactive species ( $\cdot$ OH radicals) in the aqueous reaction medium with an increase in the concentrations of the reagents [9]. However, when reaching a certain limit of concentration for the reagents, Lanox 90 removal and oxidation declines. An explanation for this phenomenon is that excess reagents might act as a scavenger of OH radicals rather than a generator [23]. It is known that hydroxyl radicals are the drivers of such oxidation removal rate. Furthermore, it can be observed from the plots that Lanox 90 elimination is extremely sensitive to the variation in pH value in the assessment of the other examined parameters. This phenomenon is in agreement with the probability values ( $p$ -values) achieved for each variable from the ANOVA test. It is important to remark that an acidic pH value is essential to conduct such oxidation.

### Numerical Optimization

Additionally, after the experimental work was conducted, the optimal results were predicted. The estimated optimal values are 854 and 0.8 mg/L for hydrogen peroxide and MMT, respectively, and the corresponding optimal pH is a pH value of 2.6 with a predicted response of 97% removal rate. Afterward, three additional replicates of the experimental work were performed to validate the predicted model, which reached a response of 98%. Thus, the numerical optimization maximized Lanox 90 oxidation, which is mainly based on OH radicals. Thus, OH radicals are increased through using the optimal reagent values and pH conditions, which exceeds the overall reaction rate.

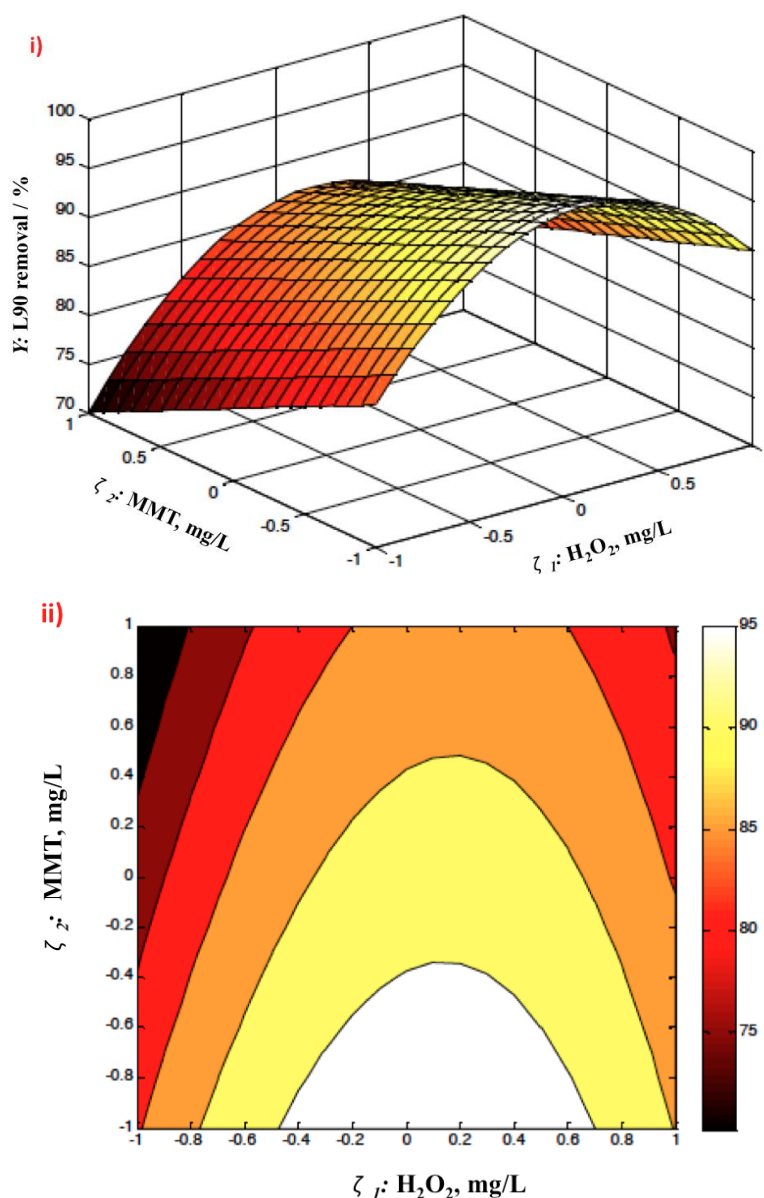


**Figure 8.** Factorial model design's optimal results: (i) 3-D surface plot and (ii) 2-D contour plot of the (Y) response and the interacting effect of H<sub>2</sub>O<sub>2</sub> and Montmorillonite catalyst concentration.

### 3.2.4. Temperature Effect on Kinetics and Thermodynamic Parameters

To proceed to real-life and practical applications, it is critical to investigate the influence of temperature on the treatment process. An investigation of the influence of temperature on reaction kinetics was conducted by changing the temperature from 26 °C (room temperature) to 40, 50, and 60 °C. The results shown in Figure 11i demonstrate that the removal rate declines to 43% as the temperature is elevated to 60 °C, when compared to a removal rate of 97% at room temperature (26 °C). Even though the oxidation reaction could be more effective at an elevated temperature, H<sub>2</sub>O<sub>2</sub> decomposes into oxygen and water at a high temperature. This results in an inhibition in the overall Lanox 90 oxidation reaction rate. Various reports in the literature [24–27] confirm the small terminal effect of reaction rate in comparison to other influencing parameters on the Fenton reaction. Some previous studies stated that 38 °C is the optimal operating temperature for the Fenton reaction [28,29].

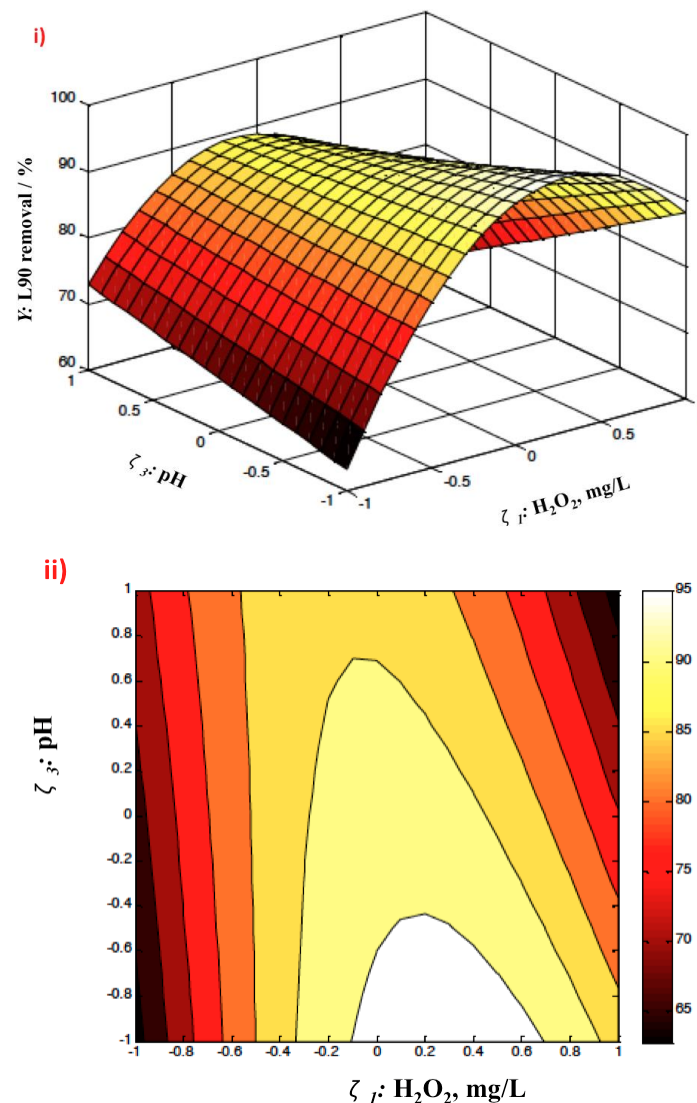


**Figure 9.** Factorial model design's optimal results: (i) 3-D surface plot and (ii) 2-D contour plot of the (Y) response and the interacting effect of H<sub>2</sub>O<sub>2</sub> and pH.

To investigate the impact of the Lanox 90 oxidation system, kinetic modeling study is essential to define the reaction rate constants. At various operating temperatures for the Montmorillonite-based Fenton system, the empirical and theoretical values of the zero-, first-, and second-order kinetic models were assessed and compared using the linearized form of Equations (1)–(3). Then, the correlation coefficient of determination values ( $R^2$ ) were compared and used to estimate the best-fit model. Commonly, the best-fit model is associated with the highest  $R^2$  value between the empirical and theoretical data [30,31]. Thus, the correlation was compared, and the zero- and first-order models were rejected for having lower  $R^2$  values, which displayed values of 0.61 to 0.88, respectively. The highest  $R^2$  value corresponds to the second-order kinetic model (0.91–0.98), as seen in Table 4. Hence, this model is selected to represent the data. This model specifies the reaction between Lanox 90 and the MMT-based photo-Fenton system, indicating that the reaction between Lanox 90 and the reagents is temperature dependent. The second-order model shows that it is not affected so much by random errors [32]. Furthermore, the half-life time ( $t_{1/2}$ ), as displayed in Table 4, increases with an increase in the temperature. This could be attributed to the increase in temperature hindering the catalytic activity of the MMT substance since its surface activity is affected by the temperature change [32,33].

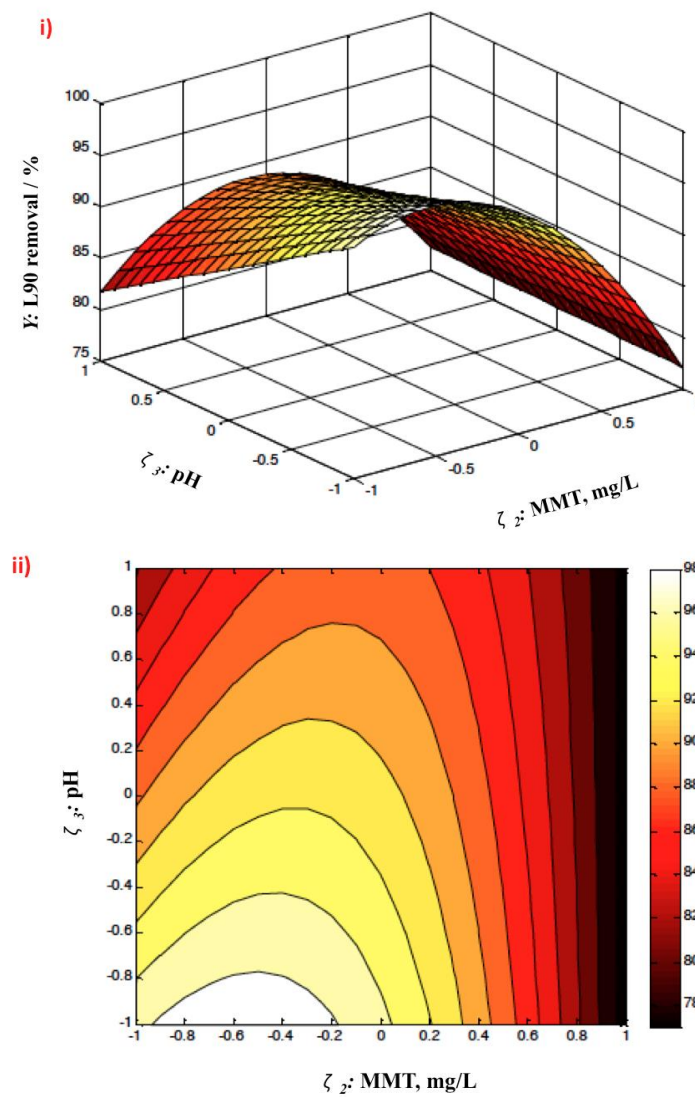


Figure 10. Factorial model design's optimal results: (i) 3-D surface plot and (ii) 2-D contour plot of the (Y) response and the interacting effect of Montmorillonite catalyst concentration and pH.

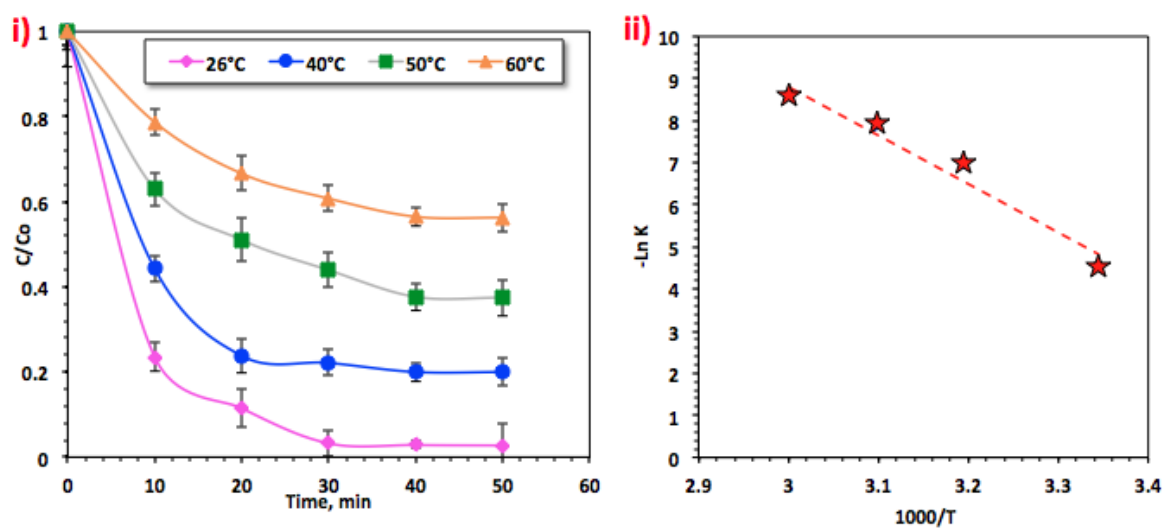


Figure 11. Effect of temperature on the reaction: (i) effect of temperature on the aqueous matrix in the photo-Fenton system, and (ii) plot of  $(-\ln K)$  vs.  $1000/T$ .

**Table 4.** Fitted kinetic reaction data for agricultural effluent oxidation reaction \*.

Kinetic Oder-Model	Boundaries	Temperature			
		299 K	313 K	323 K	333 K
Zero-order	$k_0$ (min <sup>-1</sup> )	1.48	1.33	1.11	0.82
	$t_{1/2}$ (min)	31.45	36.89	44.24	60.12
	$R^2$	0.61	0.64	0.78	0.84
First-order	$k_1$ (min <sup>-1</sup> )	0.073	0.03	0.019	0.011
	$t_{1/2}$ (min)	61.32	36.86	23.1	9.49
	$R^2$	0.88	0.76	0.88	0.88
Second-order	$k_2$ (L·mg <sup>-1</sup> min <sup>-1</sup> )	0.0101	0.001	0.0004	0.0002
	$t_{1/2}$ (min)	1.06	10.18	25.46	50.93
	$R^2$	0.91	0.92	0.99	0.98

\*  $k_0$ ,  $k_1$ , and  $k_2$ : kinetic rate constants of the zero-, first-, and second-order kinetic models;  $C_0$  and  $C_t$ : Lanox 90 loadings at initial time and time  $t$ ;  $t$ : time;  $R^2$ : coefficient of determination; and  $t_{1/2}$ : half-life time.

To further examine the influence of temperature on the Lanox 90 treatments, thermodynamic values of activation were evaluated using the Arrhenius equation (Equation (8)):

$$\ln k_2 = \ln A - \frac{E_a}{RT} \quad (8)$$

where  $A$  is the pre-exponential factor constant;  $R$  is the universal gas constant based on the second-order kinetic model used to estimate the energy of activation; and  $E_a$  is from the linear plot of  $\ln k_2$  versus  $1/T$  (Figure 11ii). Furthermore, the thermodynamic activation parameters of oxidation were estimated by using the Eyring equation (Equation (9)):

$$k_F = \frac{k_B T}{h} e^{(-\frac{\Delta G^\ddagger}{RT})} \quad (9)$$

where  $k_B$  and  $h$  are the Boltzmann and Planck's constants. Additionally, the enthalpy ( $\Delta H^\ddagger$ ) and the entropy ( $\Delta S^\ddagger$ ) of activation could be determined from the following equations [24]:

$$\Delta H^\ddagger = E_a - RT \quad (10)$$

$$\Delta S^\ddagger = (\Delta H^\ddagger - \Delta G^\ddagger) / T \quad (11)$$

The results from these equations were calculated and are shown in Table 5. The positive Gibbs free energy ( $\Delta G^\ddagger > 0$ ) and the negative values of entropy ( $\Delta S^\ddagger$ ) show the non-spontaneous nature of the oxidation reaction. Additionally, the negative values of entropy verify the exothermic nature of such reaction. These results verify the decline in the degree of freedom of Lanox 90 molecules and maintain high hydroxyl radical species yield. Similar data in the literature confirm the non-spontaneous behavior of the oxidation removal test [34,35]. Additionally, the results exhibited in Table 5 show the reaction proceeds at 95.86 kJ/mol. This high activation energy of more than 40 kJ/mol demonstrates the high-energy barrier that is required to complete the oxidation reaction of Lanox 90 molecules. Such a high level of  $E_a$  (activation energy) is well matched with the results reported in previously published articles [36,37].

### 3.2.5. Comparison of Data with the Literature

A comparison of different data presented in the literature for treating Lanox 90 and the results obtained in the current investigation (Montmorillonite-based Fenton's system) was conducted, and the results are shown in Table 6. Promisingly, photo-Fenton reaction in its heterogeneous form shows almost complete oxidation rate in all examined systems. However, in the current investigation, a lower reaction time and the use of an efficient superior treatment are needed since the catalyst is a naturally abundant material. It is

noteworthy to mention that the other systems support the use of fresh iron precursor or catalyst source associated with naturally occurring, environmentally benign catalyst as in the current study. Moreover, the catalyst's sustainability supports its use in a Fenton reaction since it is a naturally occurring and abundant material and is, thus, a cost-effective substance for Lanox 90 insecticide reduction.

**Table 5.** Thermodynamic data for agricultural effluent oxidation using Montmorillonite-based photo-Fenton reaction \*.

Temperature	$E_A = 95.86 \text{ kJ/mol}$		
	$\Delta H^\#$	$\Delta S^\#$	$\Delta G^\#$
299 K	0.038	−205.12	61.33
313 K	0.036	−186.27	58.30
323 K	0.035	−178.92	57.79
333 K	0.034	−173.41	57.74

\* Activation energy ( $E_a$ ), variation in activation enthalpy  $\Delta H^\#$  (kJ/mol), variation in activation entropy  $\Delta S^\#$  (J/mol·K), and variation in the free energy of activation  $\Delta G^\#$  (kJ/mol).

**Table 6.** Comparison of different oxidation systems for treating Lanox 90.

Treatment Process	Effluent Characteristics and Treatment Conditions	Initiation Source	Performance Efficiency	Ref.
Montmorillonite-based Fenton's system	Catalyst: 1 g/L, H <sub>2</sub> O <sub>2</sub> : 800 mg/L, pH: 6, and 26 °C	UV	97%	Current work
Alum sludge/magnetite-modified Fenton	Catalyst: 50 mg/L, H <sub>2</sub> O <sub>2</sub> : 130 mg/L, and pH: 6	UV	99%	[20]
Silica-supported iron Fenton system	23 °C, pH 3, H <sub>2</sub> O <sub>2</sub> 0.015 M, Fe <sup>2+</sup> 5.0 × 10 <sup>−4</sup> M, and 90 min	UV	98%	[31]
Heterogeneous Fenton-like copper nanoparticle-microwave system	L90 100 ppm; n-CuO 75 mg/L, H <sub>2</sub> O <sub>2</sub> 395 mg/L, and pH 6.5	MW	91%	[38]
Heterogeneous photo-Fenton-like magnetite nanoparticles	L90 50 mg/L, pH 3, iron 40 mg/L, H <sub>2</sub> O <sub>2</sub> 50 mg/L, and 60 min	UV	90%	[37]
Catalytic photooxidation-based ZnO system	L90 16 ppm, pH 5.6, ZnO 2000 mg/L, and 240 min	UV	80%	[39]
Heterogeneous solar photo-Fenton-like system	L90 50 mg/L, pH 3, iron 44 mg/L, H <sub>2</sub> O <sub>2</sub> 52 mg/L, and 170 min	Solar energy	96.5%	[20]

### 3.2.6. Assessment of Catalytic Oxidation Cycles of Montmorillonite

The life cycle of a catalytic oxidation system is one of the most important stages to assess in catalytic reactions. MMT recyclability was investigated by recycling the MMT material after Fenton oxidation. After each use, the material was collected via filtration and subjected to repeated cleaning with distilled water three times before drying in an electric furnace (105 °C) for one hour. Then, the recovered material was further used to remove Lanox 90 from wastewater, and the final Lanox 90 residual in the wastewater was monitored to check the material's ability to treat wastewater after successive use. The initial and final amounts of Lanox 90 residual were compared to check the treatment adequacy of the material, and the removal percentage was recorded.

The data shown in Figure 12 reveal the sustainability of the material; even though the oxidation efficacy lowers from 97 to 62%, the substance could still treat Lanox 90 pollutant. However, it is noteworthy to mention that the substance becomes loaded with Lanox 90 molecules, which reduces its activity. Additionally, the activity of the material till the fourth cycle indicates its stability. These data are in accordance with the results reported in a previous study [38], which investigated a copper catalyst for successive use and the treatment efficiency reached 65% after six cycles of use in comparison to 91% for the first catalyst use. Additionally, Ashour and Tony [9] investigated the recyclability of clay material, which showed a decline in the adsorption capacity, reaching 7%, when

compared to fresh clay use. Such reduction is associated with the material being loaded with pollutants, which results in a reduction in the vacancies for adsorbing further pollutants.

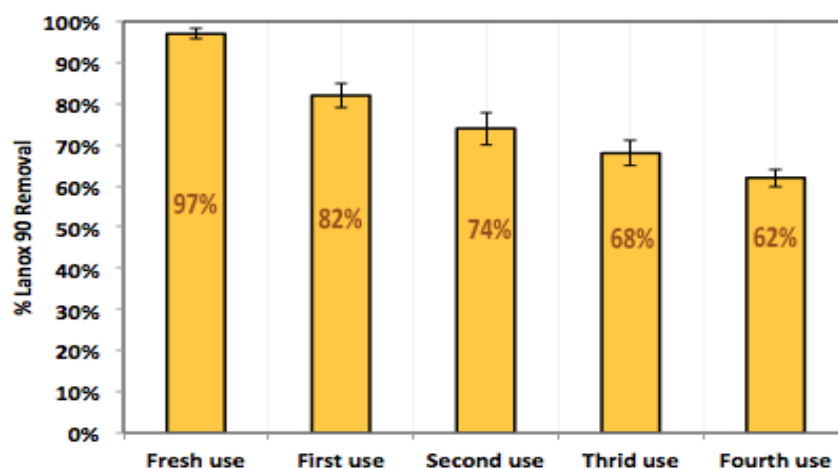


Figure 12. Catalyst's recyclability activity on Lanox 90 oxidation.

Furthermore, the dissolution of the MMT clay was investigated at an acidic pH value (2.6), and the concentrations of aluminum and iron released were recorded to be 0.043 mg/L and 0.11 mg/L, respectively. Additionally, the amount of catalyst loss after one cyclic use was estimated to be 1.02%.

#### 4. Conclusions

The present investigation reports for the first time the ability to use Montmorillonite (MMT), a naturally occurring material, to be a source of mineral for photocatalytic reaction. This study introduces its potential for agricultural wastewater reclaiming and recycling for further irrigation option. The results demonstrated that 97% of Lanox 90 could be removed from the aqueous medium using the optimized operating parameters achieved by the response surface methodology at the concentration of 854 and 0.8 mg/L for H<sub>2</sub>O<sub>2</sub> and MMT, respectively, at a pH of 2.6. The catalyst's recyclability showed a reasonable activity, reaching 62% after the fourth reuse. The kinetic investigation revealed that the reaction acted according to the second-order reaction rate. The thermodynamic parameters were categorized as exothermic and followed a non-spontaneous nature. Additionally, the reaction was conducted at a high-energy barrier. The promising results of the present work can lead to the introduction of such a system to real-life world for an environmental symbiosis approach.

**Author Contributions:** Conceptualization, E.A.H. and M.A.T.; methodology, E.A.H., M.A.T., H.A.N. and M.M.A.; software, H.A.N. and M.M.A.; validation, E.A.H. and M.A.T.; investigation, E.A.H., M.A.T., H.A.N. and M.M.A.; resources E.A.H., M.A.T., H.A.N. and M.M.A.; writing—original draft preparation, E.A.H., M.A.T., H.A.N. and M.M.A.; writing—review and editing, E.A.H., M.A.T., H.A.N. and M.M.A.; project administration E.A.H. All authors have read and agreed to the published version of the manuscript.

**Funding:** Prince Sattam Bin Abdulaziz University for funding this research work through the project number (PSAU/2022/01/23497).

**Data Availability Statement:** Data are available upon request.

**Acknowledgments:** The authors thank the Prince Sattam Bin Abdulaziz University for funding this research work through the project number (PSAU/2022/01/23497).

**Conflicts of Interest:** The authors declare no conflict of interest.

## References

1. Petchwattana, N.; Naknaen, P.; Narupai, B. A circular economy use of waste wood sawdust for wood plastic composite production: Effect of bio-plasticiser on the toughness. *Int. J. Sustain. Eng.* **2020**, *13*, 398–410. [[CrossRef](#)]
2. Wu, J.; Ding, T.; Sun, J. Neurotoxic potential of iron oxide nanoparticles in the rat brain striatum and hippocampus. *Neurotoxicology* **2013**, *34*, 243–253. [[CrossRef](#)] [[PubMed](#)]
3. Ashour, E.A.; Tony, M.A.; Purcell, P.J. Use of agriculture-based waste for basic dye sorption from aqueous solution: Kinetics and isotherm studies. *Am. J. Chem. Eng.* **2014**, *2*, 92. [[CrossRef](#)]
4. Tony, M. Win-win wastewater treatment to sustain world: Porous adsorbents from waste waterworks sludge for phenol remediation. In Proceedings of the Anaerobic Digestion Conference AD16, Delft, The Netherlands, 23–27 June 2019; The International Water Association, IWA: London, UK, 2019.
5. Gu, L.; Zhu, N.; Guo, H.; Huang, S.; Lou, Z.; Yuan, H. Adsorption and Fenton-like degradation of naphthalene dye intermediate on sewage sludge derived porous carbon. *J. Hazard. Mater.* **2013**, *246–247*, 145–153. [[CrossRef](#)]
6. Phan, T.T.N.; Nikoloski, A.N.; Bahri, P.A.; Li, D. Facile fabrication of perovskite-incorporated hierarchically mesoporous/macroporous silica for efficient photoassisted-Fenton degradation of dye. *Appl. Surf. Sci.* **2019**, *491*, 488–496. [[CrossRef](#)]
7. Nour, M.M.; Tony, M.A.; Nabwey, H.A. Immobilization of magnetic nanoparticles on cellulosic wooden sawdust for competitive Nudrin elimination from environmental waters as a green strategy: Box-Behnken Design optimization. *Int. J. Environ. Res. Public Health* **2022**, *19*, 15397. [[CrossRef](#)]
8. Nguyen, T.T.; Huynh, K.A.; Padungthon, S.; Pranudta, A.; Amonpattaratkit, P.; Tran, L.B.; Phan, P.T.; Nguyen, N.H. Synthesis of natural flowerlike iron-alum oxide with special interaction of Fe-Si-Al oxides as an effective catalyst for heterogeneous Fenton process. *J. Environ. Chem. Eng.* **2021**, *9*, 105732. [[CrossRef](#)]
9. Ashour, E.A.; Tony, M.A. Eco-friendly removal of hexavalent chromium from aqueous solution using natural clay mineral: Activation and modification effects. *SN Appl. Sci.* **2020**, *2*, 2042. [[CrossRef](#)]
10. Elsayed, S.A.; El-Sayed, I.E.; Tony, M.A. Impregnated chitin biopolymer with magnetic nanoparticles to immobilize dye from aqueous media as a simple, rapid and efficient composite photocatalyst. *Appl. Water Sci.* **2022**, *12*, 252. [[CrossRef](#)]
11. Ling, Y.; Long, M.; Hu, P.; Chen, Y.; Huang, J. Magnetically separable core-shell structural  $\gamma\text{-Fe}_2\text{O}_3\text{/Cu/Al-MCM-41}$  nanocomposite and its performance in heterogeneous Fenton catalysis. *J. Hazard. Mater.* **2014**, *264*, 195–202. [[CrossRef](#)]
12. Tireli, A.A.; Guimarães, I.D.R.; Terra, J.C.D.S.; da Silva, R.R.; Guerreiro, M.C. Fenton-like processes and adsorption using iron oxide-pillared clay with magnetic properties for organic compound mitigation. *Environ. Sci. Pollut. Res.* **2015**, *22*, 870–881. [[CrossRef](#)]
13. Van der Marel, H.W.; Beutelspacher, H. Atlas of Infrared Spectroscopy of Clay Minerals and Their Admixtures. Elsevier Publishing Company: Amsterdam, The Netherlands, 1976.
14. Tinti, A.; Tugnoli, V.; Bonora, S.; Francioso, O. Recent applications of vibrational mid-Infrared (IR) spectroscopy for studying soil components: A review. *J. Central Eur. Agric.* **2015**, *16*, 141299. [[CrossRef](#)]
15. Bukalo, N.N.; Ekosse, G.-I.E.; Odiyo, J.O.; Ogola, J.S. Fourier transform infrared spectroscopy of clay size fraction of cretaceous-tertiary kaolins in the Douala sub-basin, Cameroon. *Open Geosci.* **2017**, *9*, 407–418. [[CrossRef](#)]
16. Vaculikova, L.; Plevova, E. Identification of clay minerals and micas in sedimentary rocks. *Acta Geodyn. Geomater.* **2005**, *2*, 163.
17. Tony, M.A.; Lin, L.-S. Performance of acid mine drainage sludge as an innovative catalytic oxidation source for treating vehicle-washing wastewater. *J. Dispers. Sci. Technol.* **2021**, *43*, 50–60. [[CrossRef](#)]
18. Nassar, M.Y.; Ahmed, I.S.; Samir, I. A novel synthetic route for magnesium aluminate ( $\text{MgAl}_2\text{O}_4$ ) nanoparticles using sol-gel auto combustion method and their photocatalytic properties. *Spectrochim. Acta Part A Mol. Biomol. Spectrosc.* **2014**, *131*, 329–334. [[CrossRef](#)]
19. Nassar, M.Y.; Abdelrahman, E.A. Hydrothermal tuning of the morphology and crystallite size of zeolite nanostructures for simultaneous adsorption and photocatalytic degradation of methylene blue dye. *J. Mol. Liq.* **2017**, *242*, 364–374. [[CrossRef](#)]
20. Thabet, R.H.; Fouad, M.K.; Ali, I.A.; El Sherbiny, S.A.; Tony, M.A. Synthesis, characterization and potential application of magnetized nanoparticles for photocatalysis of Levafix CA reactive azo-dye in aqueous effluent. *Water Environ. J.* **2022**, *36*, 245–260. [[CrossRef](#)]
21. Tony, M.A.; Lin, L.-S. Iron coated-sand from acid mine drainage waste for being a catalytic oxidant towards municipal wastewater remediation. *Int. J. Environ. Res.* **2021**, *15*, 191–201. [[CrossRef](#)]
22. Tony, M.A. An industrial ecology approach: Green cellulose-based bio-adsorbent from sugar industry residue for treating textile industry wastewater effluent. *Int. J. Environ. Anal. Chem.* **2021**, *101*, 167–183. [[CrossRef](#)]
23. Guanghua, W.; Dong, W.; Wenbing, L.; Yunzhou, L.; Kun, C. Synthesis, characterization and Fenton-like degradation for Orange II of magnetic bentonite. *Chin. J. Environ. Eng.* **2014**, *8*, 1857–1862.
24. Ahmadi, M.; Behin, J.; Mahnam, A.R. Kinetics and thermodynamics of peroxydisulfate oxidation of Reactive Yellow 84. *J. Saudi Chem. Soc.* **2016**, *20*, 644–650. [[CrossRef](#)]
25. Toosi, F.S.; Hosseiny, M.; Joghataei, A.; Toosi, F.S. The Application of  $\text{SiO}_2$  Nanoparticles for Anionic Dye Removal from Aqueous Solution. *Arch. Hyg. Sci.* **2017**, *6*, 136–144.
26. Buthiyappan, A.; Raman, A.A.A.; Daud, W.M.A.W. Development of an advanced chemical oxidation wastewater treatment system for the batik industry in Malaysia. *RSC Adv.* **2016**, *6*, 25222–25241. [[CrossRef](#)]

27. Deng, Y.; Englehardt, J.D. Treatment of landfill leachate by the Fenton process. *Water Res.* **2006**, *40*, 3683–3694. [[CrossRef](#)]
28. Pintor, A.M.; Vilar, V.J.; Boaventura, R.A. Decontamination of cork wastewaters by solar-photo-Fenton process using cork bleaching wastewater as H<sub>2</sub>O<sub>2</sub> source. *Sol. Energy* **2011**, *85*, 579–587. [[CrossRef](#)]
29. Ioannou, L.A.; Fatta-Kassinos, D. Solar photo-Fenton oxidation against the bioresistant fractions of winery wastewater. *J. Environ. Chem. Eng.* **2013**, *1*, 703–712. [[CrossRef](#)]
30. Lopez-Lopez, C.; Martín-Pascual, J.; Martínez-Toledo, M.V.; González-López, J.; Hontoria, E.; Poyatos, J.M. Effect of the operative variables on the treatment of wastewater polluted with phthalo blue by H<sub>2</sub>O<sub>2</sub>/UV process. *Water Air Soil Pollut.* **2013**, *224*, 1725. [[CrossRef](#)]
31. Tony, M.A.; Lin, L.-S. Attenuation of organics contamination in polymers processing effluent using iron-based sludge: Process optimization and oxidation mechanism. *Environ. Technol.* **2022**, *43*, 718–727. [[CrossRef](#)]
32. Repo, E.; Mäkinen, M.; Rengaraj, S.; Natarajan, G.; Bhatnagar, A.; Sillanpää, M. Lepidocrocite and its heat-treated forms as effective arsenic adsorbents in aqueous medium. *Chem. Eng. J.* **2012**, *180*, 159–169. [[CrossRef](#)]
33. Singh, C.; Chaudhary, R.; Gandhi, K. Preliminary study on optimization of pH, oxidant and catalyst dose for high COD content: Solar parabolic trough collector. *Iran. J. Environ. Health Sci. Eng.* **2013**, *10*, 13. [[CrossRef](#)] [[PubMed](#)]
34. Pourali, P.; Behzad, M.; Arfaenia, H.; Ahmadfazeli, A.; Afshin, S.; Poureshgh, Y.; Rashtbari, Y. Removal of acid blue 113 from aqueous solutions using low-cost adsorbent: Adsorption isotherms, thermodynamics, kinetics and regeneration studies. *Sep. Sci. Technol.* **2021**, *56*, 3079–3091. [[CrossRef](#)]
35. Lv, Q.; Li, G.; Sun, H.; Kong, L.; Lu, H.; Gao, X. Preparation of magnetic core/shell structured  $\gamma$ -Fe<sub>2</sub>O<sub>3</sub>@ Ti-tmSiO<sub>2</sub> and its application for the adsorption and degradation of dyes. *Microporous Mesoporous Mater.* **2014**, *186*, 7–13. [[CrossRef](#)]
36. Sidney Santana, C.; Nicodemos Ramos, M.D.; Vieira Velloso, C.C.; Aguiar, A. Kinetic evaluation of dye decolorization by Fenton processes in the presence of 3-hydroxyanthranilic acid. *Int. J. Environ. Res. Public Health* **2019**, *16*, 1602. [[CrossRef](#)]
37. Chen, J.; Zhu, L. Heterogeneous UV-Fenton catalytic degradation of dyestuff in water with hydroxyl-Fe pillared bentonite. *Catal. Today* **2007**, *126*, 463–470. [[CrossRef](#)]
38. Tony, M.A.; Mansour, S.A. Microwave-assisted catalytic oxidation of methomyl pesticide by Cu/Cu<sub>2</sub>O/CuO hybrid nanoparticles as a Fenton-like source. *Int. J. Environ. Sci. Technol.* **2020**, *17*, 161–174. [[CrossRef](#)]
39. Tomašević, A.; Mijin, D.; Gašić, S.; Kiss, E. The influence of polychromatic light on methomyl degradation in TiO<sub>2</sub> and ZnO aqueous suspension. *Desalination Water Treat.* **2014**, *52*, 4342–4349. [[CrossRef](#)]

**Disclaimer/Publisher's Note:** The statements, opinions and data contained in all publications are solely those of the individual author(s) and contributor(s) and not of MDPI and/or the editor(s). MDPI and/or the editor(s) disclaim responsibility for any injury to people or property resulting from any ideas, methods, instructions or products referred to in the content.